

Linear-scaling implementation of exact exchange using the density matrix: method and accuracy

Lionel A. Truflandier¹ and David R. Bowler^{1, a)}

*London Centre for Nanotechnology and Department of Physics and Astronomy University College London
17-19 Gordon Street, London WC1H 0AH, UK*

(Dated: 15 November 2018)

In this work we consider the enhancement of the computational efficiency in exact exchange calculation using the density matrix and local support functions. We introduce a numerical method which avoids the explicit calculation the four-center electron repulsion integrals (ERIs) and reduces the prefactor scaling by a factor M , where M is the number atoms within the range of the exact exchange Hamiltonian. This approach, which uses three-center reduction integrals, takes advantage of a discrete grid which enables a direct summation over the support functions in a localized space. Using the sparsity property of the density matrix, the scaling of the prefactor can be further reduced to reach asymptotically $O(M)$. Influence of the fast Fourier transform and real space Poisson solver upon the ERI accuracy is discussed. Finally, various factors influencing the performance of the algorithm are investigated in terms of execution time and memory usage.

PACS numbers: 71.15.Ap 71.15.Mb 71.15.Dx 02.60.Jh

I. INTRODUCTION

The exchange interaction is a fundamental concept in the description and the interpretation of electronic structure of molecules and solids. Its genuine representation is found in the so-called ‘‘Fock-exchange’’ for Hartree-Fock (HF) and correlated wave-function approaches and ‘‘exact-exchange’’ for Kohn-Sham (KS) density functional theory (DFT). Unfortunately, the expensive computational resources needed for the evaluation of the exchange energy represent a serious bottleneck. This can be partially circumvented thanks to the development of elaborated integral evaluation methodologies.¹ Using the sparse density matrix techniques,² our purpose is to develop a scheme for computing exact exchange which fulfils the linear-scaling requirement, i.e. the computer effort scales linearly with the number of atoms, and as far as possible, minimizes the prefactor.

The two particle density matrix is formally defined in terms of the one-electron eigenstates as,

$$\rho(\mathbf{r}, \mathbf{r}') = \sum_n f_n \psi_n(\mathbf{r}) \psi_n^*(\mathbf{r}') \quad (1)$$

where f_n is the occupation number and n run over the doubly occupied electronic states. Traditional quantum chemistry methods approximate ψ_n by a truncated linear combination of real atom-centered functions $\{\phi_{i\alpha}\}$ —also called basis or support functions. As a result, $\rho(\mathbf{r}, \mathbf{r}')$ is finite and separable; this approach is also the basis for many linear scaling methods^{2,3}. The density kernel K is then expressed in the representation of the basis states with,

$$\rho(\mathbf{r}, \mathbf{r}') = \sum_{i\alpha j\beta} \phi_{i\alpha}(\mathbf{r}) K_{i\alpha j\beta} \phi_{j\beta}(\mathbf{r}') \quad (2)$$

where the index α runs over of the number of support functions for each atom i . For sake of simplicity, hereafter we will omit the index α . The formal expressions of the Hartree (also called Coulomb) and exchange energies are

$$J = \int \int d\mathbf{r} d\mathbf{r}' \frac{\rho(\mathbf{r}) \rho(\mathbf{r}')}{|\mathbf{r} - \mathbf{r}'|}, \quad (3)$$

$$X = \int \int d\mathbf{r} d\mathbf{r}' \frac{\rho(\mathbf{r}, \mathbf{r}') \rho(\mathbf{r}', \mathbf{r})}{|\mathbf{r} - \mathbf{r}'|}, \quad (4)$$

with $\rho(\mathbf{r}) = \rho(\mathbf{r}, \mathbf{r}')|_{\mathbf{r}=\mathbf{r}'}$ the usual electronic density. The corresponding matrix elements are given by

$$J_{ij} = \sum_{kl} (ij|kl) K_{kl} \quad (5)$$

$$X_{ij} = \sum_{kl} (ik|lj) K_{kl}, \quad (6)$$

where the 4-center integral $(ab|cd)$ related to the orbital-product density

$$\rho_{ab}(\mathbf{r}) = \phi_a(\mathbf{r}) \phi_b(\mathbf{r}), \quad (7)$$

is a short notation for the Coulomb-type integral,

$$(ab|cd) = \int \int d\mathbf{r} d\mathbf{r}' \rho_{ab}(\mathbf{r}) \vartheta(\mathbf{r}, \mathbf{r}') \rho_{cd}(\mathbf{r}'). \quad (8)$$

To simplify the notation we wrote the two-particle Coulomb operator $\vartheta(\mathbf{r}, \mathbf{r}') = |\mathbf{r} - \mathbf{r}'|^{-1}$. At a first glance, we notice that the evaluation of the 4-center electron repulsion integrals (ERIs) in Eq. (5) and Eq. (6) scales formally as N^2 , i.e. evaluation of the energy scales as N^4 , where N is the product of the number of atoms with the number of basis functions. This observation is especially true if one use atom centered Gaussian- or Slater- type orbitals (GTO and STO, respectively) and analytic or semi-analytic integration techniques. Several elaborated methods based on 3-center reductions⁴ have been introduced to alleviate the N^4 barrier of the Coulomb,⁵ and

^{a)} Electronic mail: david.bowler@ucl.ac.uk

exchange matrix calculation.^{6–9} They generally derived from the density–fitting approach of Baerends and Roos for STOs,¹⁰ and Dunlap and coworkers^{11,12} for GTO basis sets: $\rho_{ab}(\mathbf{r})$ is approximated by a model density $\tilde{\rho}(\mathbf{r})$ defined as a linear combination of atom centered auxiliary fit functions. The coefficients of the expansion are then optimized using a ‘‘Coulomb–weighted’’ constrained least squares fit method.⁵ Finally, the 3–center integrals of the kind,

$$(ab|A) = \int \int d\mathbf{r}d\mathbf{r}' \rho_{ab}(\mathbf{r})\vartheta(\mathbf{r},\mathbf{r}')\rho_A(\mathbf{r}') \quad (9)$$

are numerically evaluated with a quadrature scheme,^{13–15} or further reduced to 2–center,^{9,16} and integrated analytically.^{17,18} Different approaches which keep a similar spirit as the pseudo–spectral^{19,20} or the resolution of identity methods^{21,22} have also demonstrated to be efficient, and improvements are still explored by many groups.^{4,23,24} All of the above methods exhibit N^3 scaling, which asymptotically reach $O(N^2)$ or even $O(N)$ for the most elaborated,⁴ including fast multipole developments.^{25–27} Obviously, in this case the prefactor and the data storage become the relevant parameters to probe the real efficiency of the implementation.

Whereas GTO– and STO–based quantum chemistry approaches involved ERIs for computing the Coulomb energy, periodic DFT methods based on plane wave (PW) expansion of the KS orbitals integrate directly Eq 3 in reciprocal space using 3D–FFT algorithm. In this case, the associated computational effort of $n \times N_G \log(N_G)$,²⁸ where N_G is the number of PWs, becomes insignificant compared to the orthogonalisation or diagonalisation steps which asymptotically reach as $O(N^3)$. Using efficient parallelization of the FFT routines, reasonable scaling properties are obtained which are rapidly spoiled when the system size exceeds few hundred atoms.² This is especially true when exact–exchange is incorporated in the KS–DFT formalism.²⁹ In that case, as previously discussed for quantum chemistry methods, the evaluation of Eq. (8) for each orbital–product ρ_{ab} raises the computational cost to $n^2 \times N_G \ln(N_G)$ and asymptotically to $O(N^3)$.³⁰

Linear–scaling DFT especially developed for modern high–performance computer (HPC) is promising if one wants to perform electronic structure calculation on thousands or hundred thousands of atoms.³¹ Among the various linear scaling and support function schemes,^{2,32} real space methods based on numerical atom–centered basis functions, i.e. numerical atomic orbital (NAO) or pseudo atomic orbitals (PAO) when the pseudopotential approximation is also involved, are widely used for $O(N)$ simulations,³³ as well as in more standard approaches.³⁴ The NAOs are expressed as a linear combination of products of radial functions (f^l) and real spherical harmonic (Y_l^m),

$$\phi_i(\mathbf{r}) = \sum_{\zeta} c_{i\zeta} \varphi_{i\zeta}(\mathbf{r}) \quad (10)$$

$$\text{with } \varphi_{i\zeta}(\mathbf{r}) \equiv \varphi_{i\zeta}^{lm}(\mathbf{r}) = f_{i\zeta}^l(r) Y_l^m(\theta, \gamma) \quad (11)$$

with $\{m, l\}$ the usual quantum number. As in GTO– or STO–based quantum chemistry programs, variational flexibility can be improved by splitting the valence shell basis into multiple– ζ radial functions, and further by adding extra angular momentum components. The non–orthogonal basis set of NAOs is generated in such way that the functions are confined within a localization region of radius r_c . The NAO basis sets present various advantages: (i) The strictly localized character of these functions removes extended tails and results in sparse matrices. (ii) They are chemically intuitive since all basis functions are centered on atoms. (iii) Fast semi–numerical integral calculations are possible using spherical Bessel transform (SBT) for the radial part, and traditional analytic integration for the spherical harmonic part. In this context, Talman^{35–37} Toyoda and Ozaki^{38,39} have proposed efficient semi–numerical methods for the computation of the the 4–center ERIs. Using improved fast–SBT transform,⁴⁰ a remarkable accuracy is reached compared to full analytical results with a reasonable computational cost.³⁸ Recently, Shang et al. have introduced an fully numerical scheme.⁴¹ Each 4–center ERI is computed by evaluating the pair–density potential,

$$v_{cd}(\mathbf{r}) = \int \vartheta(\mathbf{r},\mathbf{r}')\rho_{cd}(\mathbf{r}')d\mathbf{r}' \quad (12)$$

followed by the integration in real space,

$$(ab|cd) = \int \rho_{ab}(\mathbf{r})v_{cd}(\mathbf{r})d\mathbf{r}. \quad (13)$$

The potential v_{cd} is accurately evaluated thanks to the real space Poisson solver developed by Genovese et al.^{42,43} In the same way, but using maximally localized Wannier basis functions, Wu et al. have proposed to compute v_{cd} by directly solving Poisson’s equation,

$$\nabla^2 v_{cd}(\mathbf{r}) = -4\pi\rho_{cd}(\mathbf{r}). \quad (14)$$

Discretization of the Laplace operator allows to transform Eq. (14) into a linear set of finite–difference equations which are solved using a conjugate gradient algorithm.^{44,45}

In this work, we will introduced a numerical method which enables the computation of the exchange matrix elements with a 3–center reduction integral (3CRI) scheme similar to Eq. (9); we stress that the method can be used with *any* basis set for the support functions, though we will use NAOs. The method combined the full evaluation of the basis functions on a grid with Poisson’s equation solver, as proposed by Shang et al.⁴¹ Nevertheless, here we will circumvent explicit calculations of the ERIs without any approximation. The resulting scaling is driven by a prefactor proportional to M^3 , where M is the number atoms within the range of the exact–exchange Hamiltonian, and reach asymptotically $O(M)$. The accuracy of method with respect to various FFT–based methodologies used for evaluate the pair–density potential will be

discussed. The implementation of the 3CRI approach within the architecture of DFT linear-scaling code CONQUEST will be presented in a forthcoming article.

II. 3-CENTER REDUCTION INTEGRALS

The principle of the method is straightforward: If the configuration space spanned by the support functions is described by an evenly spaced discrete basis, from the double sum of Eq. (6) recasts as

$$X_{ij} = \sum_k (ik|\vartheta \sum_l |lj) K_{kl}, \quad (15)$$

we can decompose the double sum above into a first the sum over the states l , and evaluate the exchange matrix elements through a second sum over k ,

$$X_{ij} = \sum_k (ik|\bar{v}_{kj}). \quad (16)$$

The operator \bar{v}_{kj} is no more that the “local” pair potential associated to the reduced density weighted by the density matrix coefficient,

$$\bar{\rho}_{kj} = \sum_l K_{kl} \rho_{lj}. \quad (17)$$

As a result, the exchange matrix elements are deduced from 3-center 3-dimensional Coulomb integrals. To describe the practical implementation we have to start from the explicit definition of the exchange matrix elements with respect to the ERIs and the basis set $\{\phi_a\}$. Within the discretized space, combining Eq. (6), (7) and (8), we obtain:

$$X_{ij} = \sum_{kl} K_{kl} \sum_{hg} \phi_i(\mathbf{r}_h - \mathbf{R}_i) \phi_k(\mathbf{r}_h - \mathbf{R}_k) \vartheta(\mathbf{r}_h, \mathbf{r}_g) \times \phi_l(\mathbf{r}_g - \mathbf{R}_l) \phi_j(\mathbf{r}_g - \mathbf{R}_j) w(\mathbf{r}_h) w(\mathbf{r}_g) \quad (18)$$

where we made explicit the fact that the support functions are centered on the nuclei positions $\{\mathbf{R}_a\}$. The sets $\{w(\mathbf{r}_h)\}$ and $\{w(\mathbf{r}_g)\}$ account for the weight factors of the quadrature points $\{\mathbf{r}_h\}$ and $\{\mathbf{r}_g\}$. We choose to work with an evenly spaced cubic grid where both $w(\mathbf{r}_h)$ and $w(\mathbf{r}_g)$ simplify to $w_{\text{int}} = h_{\text{int}}^3$, with h_{int} the grid spacing.⁴⁶ Under the translation $\mathbf{r} \rightarrow \mathbf{r} + \mathbf{R}_i$, which leaves invariant the ERIs, we obtain

$$X_{ij} = \sum_{kl} K_{kl} \sum_{hg} \phi_i(\mathbf{r}_h) \phi_k(\mathbf{r}_h - \mathbf{R}_{ki}) \vartheta(\mathbf{r}_h, \mathbf{r}_g) \times \phi_l(\mathbf{r}_g - \mathbf{R}_{li}) \phi_j(\mathbf{r}_g - \mathbf{R}_{ji}) w_{\text{int}}^2, \quad (19)$$

using $\mathbf{R}_{ab} = \mathbf{R}_a - \mathbf{R}_b$. By virtue of the linearity of discretized space, we are allow to introduce the temporary matrix:

$$\Phi_k(\mathbf{r}_g; \{\mathbf{R}_{li}\}) = \sum_l K_{kl} \phi_l(\mathbf{r}_g - \mathbf{R}_{li}). \quad (20)$$

We emphasize that ϕ_l is evaluated on a cubic grid centered on the nucleus i . The explicit expression for the reduced density of Eq. (17) is given by

$$\bar{\rho}_{kj}(\mathbf{r}_g; \mathbf{R}_{ji}, \{\mathbf{R}_{li}\}) = \Phi_k(\mathbf{r}_g) \phi_j(\mathbf{r}_g - \mathbf{R}_{ji}). \quad (21)$$

The corresponding reduced pair potential \bar{v}_{lj} is obtained by solving the Poisson equation. Finally, we introduce the temporary matrix:

$$\Omega_j(\mathbf{r}_h; \mathbf{R}_{ji}, \{\mathbf{R}_{li}\}, \{\mathbf{R}_{ki}\}) = \sum_k \phi_k(\mathbf{r}_h - \mathbf{R}_{ki}) \bar{v}_{kj}(\mathbf{r}_h), \quad (22)$$

to perform the last numerical integration yielding to the exchange matrix elements

$$X_{ij}(\mathbf{r}_h; \mathbf{R}_{ji}, \{\mathbf{R}_{li}\}, \{\mathbf{R}_{ki}\}) = \sum_h \phi_i(\mathbf{r}_h) \Omega_j(\mathbf{r}_h) w_{\text{int}}. \quad (23)$$

We voluntary made explicit the dependence of the various matrix with respect to the translation vectors $\{\mathbf{R}_{ab}\}$.

FIG. 1. Algorithm describing exchange kernel scaling as M^3 .

```

1: loop over atom  $i$ 
2:   ▷ evaluate and ▷ store  $\phi_i$ 
3:   loop over atom  $j$ 
4:     if  $R_{ji} < D_{ji}$  then
5:       ▷ evaluate and ▷ store  $\phi_j$ 
6:       loop over atom  $k$ 
7:         if  $R_{ki} < D_{ki}$  then
8:           ▷ evaluate  $\phi_k$  and ▷ store ?
9:           loop over atom  $l$ 
10:            ▷ fetch  $K_{kl}$ 
11:            if  $R_{li} < D_{li}$  then
12:              ▷ evaluate  $\phi_l$  and ▷ store ?
13:              ◊ accumulate  $\Phi_k$ 
14:            end if:  $D_{li}$ 
15:          end loop:  $l$ 
16:          ▷ calculate  $\bar{\rho}_{kj}$ 
17:          ▷ evaluate  $\bar{v}_{kj}$ 
18:          ◊ accumulate  $\Omega_j$ 
19:        end if:  $D_{ki}$ 
20:      end loop:  $k$ 
21:    end if:  $D_{ji}$ 
22:  end loop:  $j$ 
23:  ▷ integrate  $X_{ij}$ 
24: end loop:  $i$ 

```

This approach involves three main operations: (i) The projection of ϕ_i onto the discretized space, where both radial functions and spherical harmonics are evaluated on a cubic grid. (ii) The summations of Eqs. (20) and (22). (iii) The evaluation of the pair potential \bar{v}_{lj} .

The combination of local FFT grids⁴⁷ with the locality property of the NAOs easily fulfils the efficiency requirement. On each *primary* atom i a box is centered at the position \mathbf{R}_i . This box contains an ensemble of grid points called \mathcal{B}_i . For the NAO set $\{j, k, l\}$ in Eq. (19)

other boxes \mathcal{B}_a are defined and translated along the vector \mathbf{R}_{ai} . Here, we choose to work with identical cubic boxes of length $L \geq 2 \times r_c^{\max}$, where r_c^{\max} is the largest confinement radius over the whole set of contracted functions $\{\varphi_{i_c}^{lm}\}$. Considering that the quadrature of Eq. (19) is different from zero if significant overlap is deemed to exist between the four NAOs, we can first reduced the computational resources involved in (i) by defining reduced spaces as,

$$\mathcal{O}_{ai} = \mathcal{B}_a \cap \mathcal{B}_i \quad (24)$$

where \mathcal{O}_{ai} is the overlap box of ϕ_a with ϕ_i . Then the discretized functions $\{\phi_j, \phi_k, \phi_l\}$ are only evaluated for grid points common to the space span by ϕ_i . Secondly, by using the fact that the coordinate system is centered on the primary atom, we can introduced an efficient screening during the course of the calculation and reduced the computational time related to (ii) and (iii). Accumulation in the temporary matrices Φ_k and Ω_j , which are centered on atom i , is perform if and only if the distance R_{ai} between the two distribution centers is below the cutoff D_{ai} . If one consider this cutoff to be equal to $r_c^{\max}(a) + r_c^{\max}(i)$ where the two parameters defined the confinement radius of the centers a and i , then the calculation is exact in the representation space of $\{\phi_a\}$ and the conditional screening along with the overlap reduction only disable useless computations.

As shown in the algorithm of Fig. 1 the calculation time can be reduced further with a screening condition on exchange matrix elements X_{ij} . This is related to the sparsity property of $\rho(\mathbf{r}, \mathbf{r}')$,⁴⁸ and the truncation of all the operators involved in the Hamiltonian.³ Naturally, other screening techniques,¹ as the Schwarz inequality, might be incorporated in this algorithm. However, they generally rely on the computation of two-center integrals which is not computationally justify in our case. Indeed, our implementation is performed in the framework of density matrix linear-scaling techniques, where the main assumption is based on “fast decay” of the matrix elements K_{ij} at long range which implies a pre-screening process.

From the algorithm of Fig. 1 we note that the most time consuming operation, i.e. the evaluation of the reduced potential \bar{v}_{kj} (see below for timings), is performed within a 3-index loop, which contrasts with the M^4 scaling used for the accumulation of temporary matrix Φ_k . An other possibility would be to compute and store the set $\{\phi_l\}$ or (and) $\{\phi_k\}$ once reducing formally —after the first cycle— the execution time for the calculation of Φ_k to $M^3(M^2)$ but increasing the data storage by $M(M^2)$, respectively. These options will be studied later in the article. We will now address the computation of the reduced potential which is the remaining bottleneck.

III. POISSON EQUATION AND ACCURACY

There exist two main numerical approaches to evaluate the Coulomb potential related to a localized charge density distribution. We can choose to solve the Poisson equation in reciprocal space where the Laplace operator becomes diagonal and

$$\tilde{v}_{kj}(\mathbf{G}) = 4\pi \frac{\tilde{\rho}_{kj}(\mathbf{G})}{\mathbf{G}^2}. \quad (25)$$

\mathbf{G} is the reciprocal space analogue of the real space vector \mathbf{r} defined in the atom centered cubic box of volume $V = L^3$. Fourier transform of the density from real to reciprocal space

$$\tilde{\rho}_{kj}(\mathbf{G}) = \int_V d\mathbf{r} \bar{\rho}_{kj}(\mathbf{r}) e^{-i\mathbf{G}\cdot\mathbf{r}}, \quad (26)$$

and the inverse transform applied to the potential

$$\bar{v}_{kj}(\mathbf{r}) = \sum_{\mathbf{G} \neq 0} \tilde{v}_{kj}(\mathbf{G}) e^{i\mathbf{G}\cdot\mathbf{r}}, \quad (27)$$

can be performed using the FFT technologies. This second approach is the most appropriate for periodic neutral systems —when the positively charged nuclei compensate exactly the electronic charge density— it becomes less relevant for isolated and/or charged systems. When dealing with localized charge densities, the Fourier expansion of Eq. (26) leads to issues which affect dramatically the accuracy of the potential.⁴⁹ The enforced periodicity arising from the wave factor induces spurious electrostatic interactions between periodic images which are naturally magnified for charged systems. Moreover, in this case $\tilde{v}_{kj}(\mathbf{G} \rightarrow 0)$ diverges instead of converging to zero and violates the classical law $\bar{v}_{kj}(\mathbf{r} \rightarrow \infty) \approx 0$ which must be valid for any Coulomb potentials associated with isolated charges.

Several schemes have been developed to tackle this problem,⁵⁰⁻⁵² and we refer the reader to Refs. 49 and 53 for recent studies —and references therein. Alternatively, Poisson’s equation can be solved in real space. Wu et al. proposed to seek for \bar{v}_{kj} as solution of Eq. (14) by discretizing the Laplace operator in real space and solving the corresponding set of finite difference equations using a conjugate gradient algorithm.⁴⁴ An other class of method, which avoids the direct resolution of the Poisson equation is based on the discrete variable representation (DVR) of Eq. (12).⁵⁴ The density is generally expanded in a direct product of one-dimensional localized real-space basis functions as Chebyshev polynomials,⁵⁵ sinc,⁵⁴ Lagrange⁵⁶ functions, or interpolating scaling functions (ISF).⁵⁷ As a result, the potential is free of boundary conditions. The remaining issue related to the Coulomb singularity is circumvented by an integral transformation and a Gauss quadrature,⁵⁸ or by the separable formulation of the $1/r$ operator over Gaussian functions as proposed by Beylkin et al.^{59,60}

TABLE I. Deviations of numerical ERIs computed for H₂ with respect to the semi-numerical method of Toyoda et al. implemented in LIBERI.³⁹ A fixed grid spacing of 0.20 au was used for both the FFT- and DVR-based methods.

Method	κ^a	r_{int} (au)	N_g^b	Integrals (au)			
				(11 11)	(12 11)	(12 12)	(11 22)
LIBERI ^c	n/a	n/a	2048	0.6141895	0.4273042	0.3291038	0.5012347
				Deviations (au)			
				(11 11)	(12 11)	(12 12)	(11 22)
FFT/no correction ^d	2.7	12.86	129	0.1177822	0.0883207	0.0668717	0.1156119
FFT-SCC	1.2	5.65	57	0.0140899	0.0076902	0.0064139	0.0038279
	2.7	12.86	129	0.0094874	0.0065076	0.0049596	0.0076849
	8.0	37.67	377	0.0032908	0.0021934	0.0016352	0.0026264
FFT-CCC	1.2	5.65	57	-0.0005123	-0.0026848	-0.0003908	-0.0071520
	1.5	7.06	71	-0.0002621	-0.0003906	-0.0000992	-0.0047685
	2.0	9.42	95	-0.0001081	-0.0002508	-0.0000903	-0.0030707
DVR-ISF ^e	1.0	4.71	48	0.0000018	-0.0000968	-0.0001299	0.0001028

^a The relation between κ and r_{int} is given by $r_{\text{int}} = \kappa \times r_c^{\text{max}}$, where r_c^{max} is the confinement radius of the PAO.

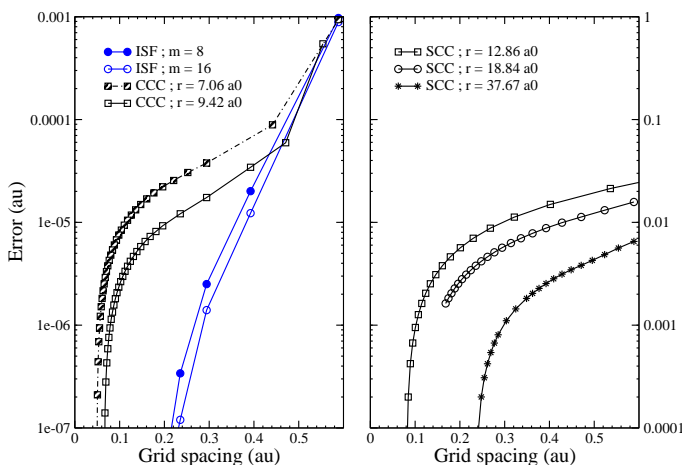
^b N_g is the number of grid points along one direction. For the SBT approach, N_g corresponds to the number of points used to discretized the radial component.

^c The convergence parameters are: (i) maximum value of angular momentum $l_{\text{max}} = 10$, (ii) $\bar{l}_{\text{max}} = 8$ and $\bar{N}_g = 180$ for the Gauss-Laguerre quadrature.³⁸

^d No correction is applied and the $\mathbf{G} = 0$ component is neglected as in Eq. (27).

^e A number of 16 interpolating scaling functions were used for the density mapping.

FIG. 2. Convergence of the numerical Coulomb-type ERI for H₂ with respect to the grid step and the Poisson solver. Left panel: with the DVR-ISF and FFT-CCC method. Right panel: with the FFT-SCC method. Influence of the scaling-order m for ISF and the integration radius for the FFT-based approaches are also demonstrated.



Later in this article we will investigate the accuracy of two FFT-based Poisson solvers: (i) The spherical cutoff of the Coulomb potential (SCC).^{52,61} The Coulomb potential is truncated at distance C where the localized

electronic density vanishes preventing undesired interactions between periodic images. It is easily demonstrated that the Fourier transform of $\tilde{v}_{kj}(\mathbf{r})$ is then given by

$$\tilde{v}_{kj}(\mathbf{G}) \approx 4\pi\tilde{\rho}_{kj}(\mathbf{G})\frac{1 - \cos(C|\mathbf{G}|)}{G^2} \quad (28)$$

In this respect the $\mathbf{G} = 0$ component of potential is finite with $\tilde{v}_{kj}(0) = 2\pi C^2$. The spherical cutoff approach and its generalization to 1D and 2D periodic system have been investigated in details elsewhere.^{49,51,62} Generally, the density cutoff is defined as $C = 2\sqrt{3} \times r_c^{\text{max}}$ and the box side length is given by $L = 2\kappa \times r_c^{\text{max}}$ with $\kappa \geq 1 + \sqrt{3}$.^{49,52} (ii) The counter charge corrections (CCC).^{49,53,63,64} At first thought, if one want to eliminate periodic-image interactions of the net charge $q_{kj} = \int_V d\mathbf{r}\tilde{\rho}_{kj}(\mathbf{r})$ which in reciprocal space are concentrated at $\mathbf{G} = 0$ and recover the useful relation $\tilde{v}_{kj}(0) = 0$, we can add to $\tilde{\rho}_{kj}$ a jellium compensating charge and correct the potential accordingly. This approach implies that the density must be very localized, or conversely that the cell is large enough to allow the approximation of $\tilde{\rho}_{kj}$ by a Dirac delta function. If now the q_{kj} is close to zero, as for a p -like or d -like charge distribution, we observe that no particular corrections are applied, and that higher order in the model have to be included if one want to correct the spurious electrostatic interactions of the nonspherical components. Then, the

second thought bring us to introduce a more general approach where the compensating model density ρ_M is expanded in a set of auxiliary densities presenting the same multipolar moments than $\bar{\rho}_{kj}$. If Gaussian functions are used for the auxiliary basis, the derivation of the correcting potential v_M can be analytical.⁴⁹ Hereafter, for sake of demonstration, we have considered a unique normalized Gaussian function centered on the origin of the cell and weighted by q_{kj} . We make sure that the tail of the Gaussian do not spill over the boundaries of the box. Then ρ_M is added to $\bar{\rho}_{kj}$ in real space. After the first FFT of Eq. (26), the potential in reciprocal space obtained through

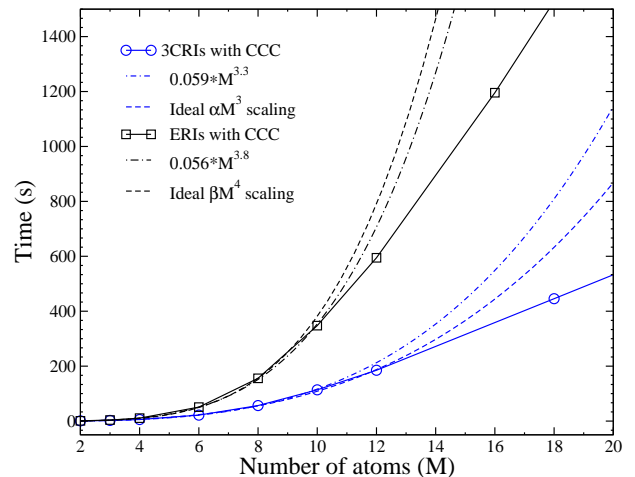
To probe the accuracy of the two FFT-based approaches and the DVR- ISF Poisson solver developed by Genovese et al.^{42,43} we have computed the four inequivalent ERIs of H_2 —with an interatomic distance of 1.4 au. A single- ζ PAO with $r_c^{\text{max}} = 4.71$ au has been used for the support functions. For the ISF Poisson solver, 89 Gaussian functions were used for the linear expansion of the Coulomb operator, as implemented in the ISF module.⁶⁵ Deviations of the numerical ERIs with respect to the results obtained with the semi-numerical SBT-method^{38–40} of Toyoda et al. are reported in Table I.

Convergence of the (11|11) ERI with respect to the grid spacing h_{int} and the integration radius r_{int} for FFT-based approaches are represented in Fig. 2. We emphasize that whereas accuracy of the DVR methods are formally independent of the range of the integration radius, i.e. the size of the box, periodic-image interactions remain for counter-charge or spherical-cutoff corrected FFT approaches.⁴⁹ As a result, whatever the scheme for the correction, larger simulation cells are always required when one applies FFT technique to solve the Poisson equation for isolated systems. This is apparent if one examine the deviations of the H_2 ERIs as a function of the integration radius —with a fixed h_{int} — for the SCC- and CCC-FFT methods (see Table I). We observe a decrease of the deviation with respect to the reference values for larger cell but the convergence of the ERIs is very slow compared to the computational effort which scales globally as N_g^3 , where N_g is the number of grid points along one direction, with $N_g^3 \log(N_g^3)$ for the FFT part (see Fig. 2). This conclusion is reinforced by the plots of Fig. 2 where a logarithmic scale is used for the errors. From Table I, we notice that CCC outperforms SCC by an order of magnitude using more reasonable computational resources, with an error below the mHa for $r_{\text{int}} = 1.2 \times r_c^{\text{max}}$. We also emphasize that if no correction is applied to the FFT-based Poisson solver, the ERIs are underestimated by 20 %.

Finally, we find that the most suitable Poisson solver to reach a fine accuracy with reasonable computational resources is the DVR- ISF , with a deviation around 10^{-4} Ha and an exponential convergence with respect to the grid spacing. Notice that, as previously demonstrated by Genovese et al.⁴² the convergence rate can be accelerated by increasing the number of interpolating functions

(see Fig. 4) without impacting the numerical effort which, like for standard FFT technique, scales as $N_g^3 \log(N_g^3)$. Eq. (27) is FFT back and the correcting potential v_M is subtracted to \bar{v}_{kj} in real space.

FIG. 3. Comparison of CPU times necessary to compute exact exchange as a function of number atoms using explicit ERI calculation and the 3CRI method. The FFT-CCC approach was used to solve the Poisson equation. Polynomial fits along with ideal M^3 and M^4 scaling are also reported (see text for details).



IV. TIMING PROPERTIES AND SCALING

Practical tests on the efficiency of the 3CRI algorithm were performed on linear chains of hydrogen atoms. This system allows us to realize fast computations and simplify the interpretation of the results, without compromising the generality of the result. Calculations were performed on 1 processor with a fixed grid spacing of 0.20 au for the PAO discretization and integration radii of 5.65 and 4.71 au for FFT-CCC and DVR- ISF , respectively. Notice that all the conclusions drawn from this 1D system is fully transferable to 3D lattices.

In Fig. 3 are reported the central processing unit (CPU) times used for the computation of exact exchange as a function of the length of the atomic chain using explicit evaluation of the ERIs and the 3CRI approach. First, we observe that above 8 atoms, i.e. for a minimum interatomic distance of 9.8 au, we reach a linear scaling regime for both approaches, which is also apparent in Fig. 4). This highlights the role of the overlap screening introduced previously (see Fig. 1). This observation is reinforced by comparing the numerical results to the ideal αM^3 and βM^4 scaling of Fig. 3 obtained from a curve fitting in the range $[0; 8]$ where only α and β were optimized. We found that the M^4 scaling prefactor β is around 3 times larger than α . Within the same range, if the polynomial fitting is fully relaxed, a scaling ratio of about $M^{0.5}$ is obtained compared to the ideal value of

FIG. 4. Comparison of CPU times necessary to compute exact exchange as a function of number atoms using FFT and DVR approaches for solving Poisson’s equation. Influence of the data storage is presented in terms of CPU time (left y -axis) and memory (right y -axis).

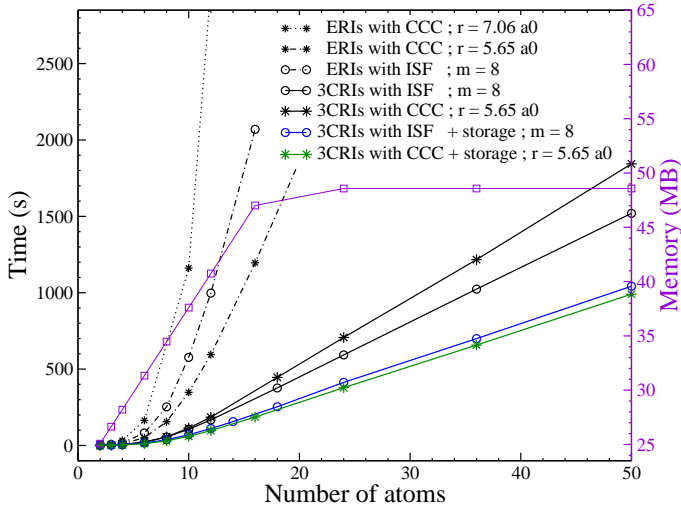
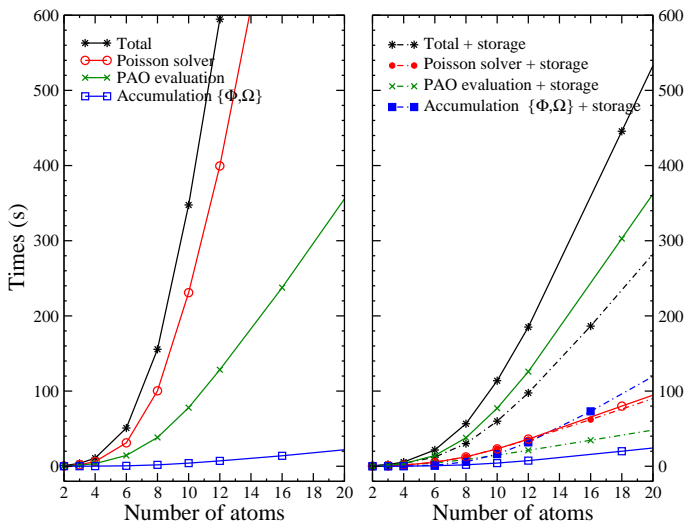


FIG. 5. Execution time decomposition with respect to the main routines involved in exact exchange calculations: the resolution of the Poisson equation, the PAO discretization and the accumulation in the temporary matrices Φ and Ω . Influence of the data storage is also presented. Left panel: with explicit evaluation of the ERIs. Right panel: using the 3CRI approach.



M . In that case the two prefactors are almost identical with a value around 0.06 s. Comparison of the FFT and DVR approach upon the CPU time is presented in Fig. 4 along with the influence of the data storage. For the ERI algorithm, we observe that FFT–CCC is faster than the real–space approach for which the size of the grid is reduced by a factor 1.73 (i.e. 1.2^3 ; see Table I). Conversely, the opposite trend is found when the 3CRI

algorithm is employed. After inspection, we found that these variations are due to the different prefactor in the FFT techniques which is also embedded in the ISF Poisson solver.⁴³

Partial storage of the PAOs (the set $\{\phi_l\}$, see line 12 of Fig. 1) leads to a net reduction of the execution time by a factor 1.8 and 1.5 for the FFT–CCC and DVR–ISF) Poisson solver, respectively. A better appreciation of the underlying factor that influence the scaling behavior is given in Fig 5. The improvement arising from the 3–center reduction algorithm is mainly located in the Poisson solver routine, which is formally called M^4 times by the ERI algorithm, compared to M^3 for 3CRI. For the sake of verification, notice that the same amount of time is spent in the PAO evaluation and the accumulation parts (see Fig. 1) of the two algorithms. As expected, the CPU time reduction observed when the partial saving of the PAOs is turn on (right panel of Fig 5) is due to the decrease by a factor of the time spend in the PAO evaluation routine. Nevertheless, there is a price to pay through a slower memory access and the noticeable increase of the accumulation time. As a rule, we are facing the eternal dilemma of data storage *vs.* execution time,^{66–68} and a good balance between both procedures must be found in order to optimize to computational resources used. Finally, we note that the data storage fulfils the linear scaling requirements as demonstrated in Fig. 4. For an evenly spaced chain of atoms as considered in this work, the saturation regime, which reaches 48.5 MB — using the computational settings describe previously—, is reasonable compared to the memory peak of 21.9 MB obtain when the data storage is bypassed.

V. CONCLUSION AND PERSPECTIVES

Using a linear combination of discrete basis set and the 3–center reduction method, we have shown that we are able to circumvent the M^4 scaling inferred by the calculation of exact exchange with the full set of ERIs. It is important to notice that the exact–exchange Hamiltonian and energy obtained with the 3CRI approach are rigorously identical to the traditional ERI results. Moreover, if the atomic–like orbitals are localized and finite range, it is further possible to achieve linear scaling in both CPU time and memory usage. We emphasize that the $O(M)$ regime obtained in this study —where M is the number atoms within the range of the exact–exchange Hamiltonian— defines the scaling behavior of the $O(N)$ density matrix techniques —where N is the total number of atoms. Within a forthcoming article we will describe the parallel implementation of exact exchange within the matrix multiplication kernel of Conquest,⁶⁹ and demonstrate that the parallelization of the 3CRI algorithm only involved exchange of the density matrix elements across processors.

ACKNOWLEDGMENTS

L.A.T. was supported by the BBSRC grant BB/H024217/1, “Linear Scaling Density Functional Theory for Biochemistry”. D.R.B. was supported by the Royal Society. The authors are grateful to L. Tong, M. J. Gillan and T. Ozaki for useful discussions.

- ¹C. Ochsenfeld, J. Kussmann, and D. S. Lambrecht, *Rev. Comput. Chem.*, **23**, 1 (2007).
- ²D. R. Bowler and T. Miyazaki, arXiv:1108.5976 (2011).
- ³E. Hernández, M. J. Gillan, and C. M. Goringe, *Phys. Rev. B*, **53**, 7147 (1996).
- ⁴R. A. Friesner, R. B. Murphy, M. D. Beachy, M. N. Ringnalda, W. T. Pollard, B. D. Dunietz, and Y. Cao, *J. Phys. Chem. A*, **103**, 1913 (2011).
- ⁵F. R. Manby, P. J. Knowles, and A. W. Lloyd, *J. Chem. Phys.*, **115**, 9144 (2001).
- ⁶R. Polly, H. Werner, F. R. Manby, and P. J. Knowles, *Mol. Phys.*, **102**, 2311 (2004).
- ⁷F. Neese, F. Wennmohs, A. Hansen, and U. Becker, *Chem. Phys.*, **356**, 98 (2009).
- ⁸M. A. Watson, N. C. Handy, and A. J. Cohen, *J. Chem. Phys.*, **119**, 6475 (2003).
- ⁹M. Krykunov, T. Ziegler, and E. van Lenthe, *Int. J. Quantum Chem.*, **109**, 1676 (2009).
- ¹⁰E. Baerends, D. Ellis, and P. Ros, *Chem. Phys.*, **2**, 41 (1973).
- ¹¹B. I. Dunlap, J. W. D. Connolly, and J. R. Sabin, *J. Chem. Phys.*, **71**, 3396 (1979).
- ¹²B. I. Dunlap, J. W. D. Connolly, and J. R. Sabin, *J. Chem. Phys.*, **71**, 4993 (1979).
- ¹³A. D. Becke and R. M. Dickson, *J. Chem. Phys.*, **89**, 2993 (1988).
- ¹⁴A. D. Becke, *J. Chem. Phys.*, **88**, 2547 (1988).
- ¹⁵V. Termath and N. C. Handy, *Chem. Phys. Lett.*, **230**, 17 (1994).
- ¹⁶F. R. Manby and P. J. Knowles, *Phys. Rev. Lett.*, **87**, 163001 (2001).
- ¹⁷S. Obara and A. Saika, *J. Chem. Phys.*, **84**, 3963 (1986).
- ¹⁸M. P. Barnett, *J. Chem. Phys.*, **113**, 9419 (2000).
- ¹⁹F. Richard A., *Chem. Phys. Lett.*, **116**, 39 (1985).
- ²⁰R. A. Friesner, *J. Chem. Phys.*, **85**, 1462 (1986).
- ²¹K. Eichkorn, O. Treutler, H. Öhm, M. Häser, and R. Ahlrichs, *Chem. Phys. Lett.*, **242**, 652 (1995).
- ²²K. Eichkorn, F. Weigend, O. Treutler, and R. Ahlrichs, *Theor. Chem. Acc.*, **97**, 119 (1997).
- ²³R. Izsák and F. Neese, *J. Chem. Phys.*, **135**, 144105 (2011).
- ²⁴S. Reine, E. Tellgren, A. Krapp, T. Krægaard, T. Helgaker, B. Jansik, S. Høst, and P. Salek, *J. Chem. Phys.*, **129**, 104101 (2008).
- ²⁵R. Kutteh, E. Aprà, and J. Nichols, **238**, 173 (1995).
- ²⁶C. A. White, B. G. Johnson, P. M. Gill, and M. Head-Gordon, *Chem. Phys. Lett.*, **253**, 268 (1996).
- ²⁷C. A. White and M. Head-Gordon, *J. Chem. Phys.*, **101**, 6593 (1994).
- ²⁸Here we consider a large enough supercell where the sampling of the first Brillouin zone reduced to the Γ -point.
- ²⁹F. Gygi and A. Baldereschi, *Phys. Rev. B*, **34**, 4405 (1986).
- ³⁰M. Marsman, J. Paier, A. Stroppa, and G. Kresse, *J. Phys.: Condens. Matter*, **20**, 064201 (2008).
- ³¹D. R. Bowler and T. Miyazaki, *J. Phys.: Condens. Matter*, **22**, 074207 (2010).
- ³²S. Goedecker, *Rev. Mod. Phys.*, **71**, 1085 (1999).
- ³³H. Shang, H. Xiang, Z. Li, and J. Yang, *Int. Rev. Phys. Chem.*, **29**, 665 (2010).
- ³⁴V. Blum, R. Gehrke, F. Hanke, P. Havu, V. Havu, X. Ren, K. Reuter, and M. Scheffler, *Comput. Phys. Comm.*, **180**, 2175 (2009).
- ³⁵J. D. Talman, *Int. J. Quantum Chem.*, **93**, 72 (2003).
- ³⁶J. D. Talman, *Int. J. Quantum Chem.*, **93**, 72 (2003).
- ³⁷J. D. Talman, *Mol. Phys.*, **108**, 3289 (2010).
- ³⁸M. Toyoda and T. Ozaki, *J. Chem. Phys.*, **130**, 124114 (2009).
- ³⁹M. Toyoda and T. Ozaki, *Comput. Phys. Comm.*, **181**, 1455 (2010).
- ⁴⁰M. Toyoda and T. Ozaki, *Comput. Phys. Comm.*, **181**, 277 (2010).
- ⁴¹H. Shang, Z. Li, and J. Yang, *J. Phys. Chem. A*, **114**, 1039 (2010).
- ⁴²L. Genovese, T. Deutsch, A. Neelov, S. Goedecker, and G. Beylkin, *J. Chem. Phys.*, **125**, 074105 (2006).
- ⁴³L. Genovese, T. Deutsch, and S. Goedecker, *J. Chem. Phys.*, **127**, 054704 (2007).
- ⁴⁴X. Wu, A. Selloni, and R. Car, *Phys. Rev. B*, **79**, 085102 (2009).
- ⁴⁵X. Wu, E. J. Walter, A. M. Rappe, R. Car, and A. Selloni, *Phys. Rev. B*, **80**, 115201 (2009).
- ⁴⁶There is no restriction for the generation of the sampling points and the corresponding weights. It is well known that other non-linear distributions allow to accelerate the convergence of numerical integration with respect to the size of the grid, mainly when we have to deal with singularities due to electronic cusps (for all-electron approaches) and Coulomb potentials. In this case, if one want to make an efficient use of FFT for the computation of coulomb potential, we have to introduced transformation matrix to map the nonlinear distributions onto the FFT grid. We let this possibility open for future investigations.
- ⁴⁷C. Skylaris, A. A. Mostofi, P. D. Haynes, C. J. Pickard, and M. C. Payne, *Comput. Phys. Comm.*, **140**, 315 (2001).
- ⁴⁸W. Kohn, *Phys. Rev. Lett.*, **76**, 3168 (1996).
- ⁴⁹A. Castro, A. Rubio, and M. Stott, *Can. J. Phys.*, **81**, 1151 (2003).
- ⁵⁰G. J. Martyna and M. E. Tuckerman, *J. Chem. Phys.*, **110**, 2810 (1999).
- ⁵¹C. A. Rozzi, D. Varsano, A. Marini, E. K. U. Gross, and A. Rubio, *Phys. Rev. B*, **73**, 205119 (2006).
- ⁵²M. R. Jarvis, I. D. White, R. W. Godby, and M. C. Payne, *Phys. Rev. B*, **56**, 14972 (1997).
- ⁵³I. Dabo, B. Kozinsky, N. E. Singh-Miller, and N. Marzari, *Phys. Rev. B*, **77**, 115139 (2008).
- ⁵⁴H. Lee and M. E. Tuckerman, *J. Chem. Phys.*, **129**, 224108 (2008).
- ⁵⁵M. A. Watson and K. Hirao, **129**, 184107 (2008).
- ⁵⁶K. Varga, Z. Zhang, and S. T. Pantelides, *Phys. Rev. Lett.*, **93**, 176403 (2004).
- ⁵⁷S. Goedecker, 1st ed. (Presses Polytechniques et Universitaires Romandes (PPUR), 1998) ISBN 2880743982.
- ⁵⁸D. Sundholm, *J. Chem. Phys.*, **122**, 194107 (2005).
- ⁵⁹G. Beylkin and L. Monzón, *Appl. Comput. Harmon. Anal.*, **12**, 332 (2002).
- ⁶⁰G. Beylkin and L. Monzón, *Appl. Comput. Harmon. Anal.*, **19**, 17 (2005).
- ⁶¹G. Onida, L. Reining, R. W. Godby, R. Del Sole, and W. Andreoni, *Phys. Rev. Lett.*, **75**, 818 (1995).
- ⁶²L. Fürti-Molnár and P. Pulay, *J. Chem. Phys.*, **117**, 7827 (2002).
- ⁶³P. E. Blöchl, *J. Chem. Phys.*, **103**, 7422 (1995).
- ⁶⁴P. A. Schultz, *Phys. Rev. B*, **60**, 1551 (1999).
- ⁶⁵<http://pages.unibas.ch/comphys/comphys/software.htm>.
- ⁶⁶J. Almlöf, K. Faegri Jr., and K. Korsell, *J. Comput. Chem.*, **3**, 385 (1982).
- ⁶⁷M. Häser and R. Ahlrichs, *J. Comput. Chem.*, **10**, 104 (1989).
- ⁶⁸P. M. W. Gill, A. T. B. Gilbert, and T. R. Adams, *J. Comput. Chem.*, **21**, 1505 (2000).
- ⁶⁹D. Bowler, T. Miyazaki, and M. Gillan, *Comput. Phys. Comm.*, **137**, 255 (2001).